Concurrent Dual-Mode Directional Coupler for Mode-Division Multiplexed Multi-Drop Substrate-Integrated Waveguide-Based Links

Mohamed Elsawaf, *Graduate Student Member, IEEE* and Constantine Sideris, *Senior Member, IEEE*

***Abstract*—This article introduces a concurrent dual-mode directional coupler design for substrate-integrated waveguides (SIWs), which can independently excite the fundamental and second higher-order modes (TE_{10} and TE_{20}). We utilize this coupler to demonstrate the possibility of creating a multi-mode, multi-drop communication link, which exploits mode orthogonality, enhancing the total channel capacity. To the best of our knowledge, this is the first realization of a concurrent multi-mode directional coupler in SIW technology. The coupling structure consists of four coupling nodes. Each one has two ports (one per mode), resulting in a total of 8 ports. The coupling factors for the TE_{10} and TE_{20} modes are -10dB each, allowing 10 drop points along the SIW in a multi-drop SIW link. The structure was fabricated using a Rogers Duroid 5880 substrate, achieving a 10-dB return loss (RL) bandwidth (BW) of more than 3.2 GHz (11.8-15 GHz) and 3.5 GHz (10-13.5 GHz) for the fundamental and second modes, respectively, corresponding to 1.7 GHz of BW for concurrent mode division multiplexing. The measured isolation between the two channels is more than 30 dB across the entire band, and the insertion loss is 1.0dB and 1.5dB, respectively. The measurement results agree well with electromagnetic simulations.**

***Index Terms*—Directional couplers, full duplex, high-speed interconnects, mode-division, multi-drop, multiplexing, substrate-integrated waveguide (SIW).**

I. Introduction

THE ever-increasing demand for faster and more efficient communication links has recently led to the evolution of the term "Terahertz (THz) links". These links target applications such as inter-rack, backplane, and fast chip-to-chip communication [1]–[4]. Such applications have a range requirement that falls below the optical fiber economical limit set by the optical/electric conversion efficiency and difficulty integrating with standard CMOS fabrication technologies. Traditional copper-based wireline links are also unsuitable for many of these applications due to their excessive losses at higher data rates. Recently, waveguide-based links, such as plastic waveguides and substrate-integrated waveguides (SIW), have garnered much attention as a potential solution for short-to-moderate distance applications that demand high data rates. Plastic waveguides provide economical, low-loss solutions for shorter length scales than fibers, e.g., fulfilling inter-rack communication requirements in large data centers. On the other hand, SIWs, which can be inexpensively realized using both chip and conventional printed circuit board (PCB) fabrication technologies, provide an efficient, low-cost, and readily integrable solution for high-speed, efficient chip-to-chip communications.

SIWs can be realized using conventional printed circuit board (PCB) technology by leveraging the PCB substrate as the dielectric guiding material, offering low-cost planar alternatives to conventional 3D bulky dielectric waveguides. SIWs inherit the low-loss and shielding properties of their 3D bulky metal-clad dielectric counterparts while significantly simplifying fabrication complexity and reducing costs. The top and bottom metals of the PCB laminate act as the waveguide floor and ceiling, while metallic posts (known as "vias"), spaced apart considerably below the smallest operating wavelength, form the side walls. Accordingly, SIWs have the same fundamental (TE_{10}) and first higher-order (TE_{20}) modes of conventional rectangular waveguides. This fundamental mode has been successfully leveraged in many SIW-based designs, ranging up to sub-THz applications, in both discrete and integrated form, including filters [5], antenna at THz frequencies [6], and at lower frequencies [7] and [8], power dividers/combiners [9], THz triplexers [10], and directional couplers [11]–[17]. In particular, waveguide directional couplers have been realized in multiple forms, including Beethe, multi-hole, and Riblet short slot couplers [18]. The first two types (Beethe and multi-hole) are created by stacking two SIWs on top of each other and opening holes in the shared metal [11] and [12]. Alternatively, the Riblet short-slot coupler has been realized by placing two SIWs next to each other and removing part of the middle via a barrier between them [15], [16]. A recent work has combined both techniques to realize a 3-dB coupler in a half-mode SIW [17].

Many recent works have also explored exciting and utilizing higher-order modes in SIWs, such as [19]–[22]. The first higher-order TE_{20} mode was excited in [19] using a slotted line fed via a microstrip to slotted line transition. On the other hand, the second higher order mode TE_{30} was excited in [22] by using a Coplanar Waveguide (CPW) transition into two slots extended along the longitudinal direction to convert the CPW mode into the TE_{30} mode. Another design that utilizes both the fundamental and the first higher-order mode excitation over different frequency bands to build a multi-channel communication link was proposed in [20]. Elsawaf and Sideris presented in [23] for the first time a concurrent multi-mode SIW channel that can be utilized to achieve full-

Manuscript received Oct. 18^{th}2023; revised Dec. 17^{th}2023; accepted Jan. 15^{th}2024. *(Corresponding author: Constantine Sideris)*. This work is funded by the National Science Foundation (CCF-2047433, ECCS-2133138). The authors are with the Department of Electrical and Computer Engineering, University of Southern California, Los Angeles, CA, 90089 USA (e-mail: elsawaf@usc.edu; csideris@usc.edu).

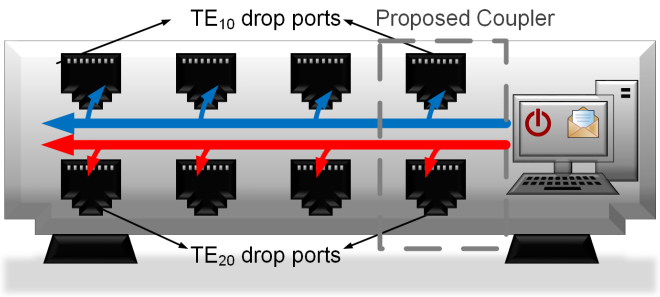

Fig. 1. A potential multi-drop multi-port system with the proposed coupler function used to double the number of peripheral drops over the same data channel highlighted.

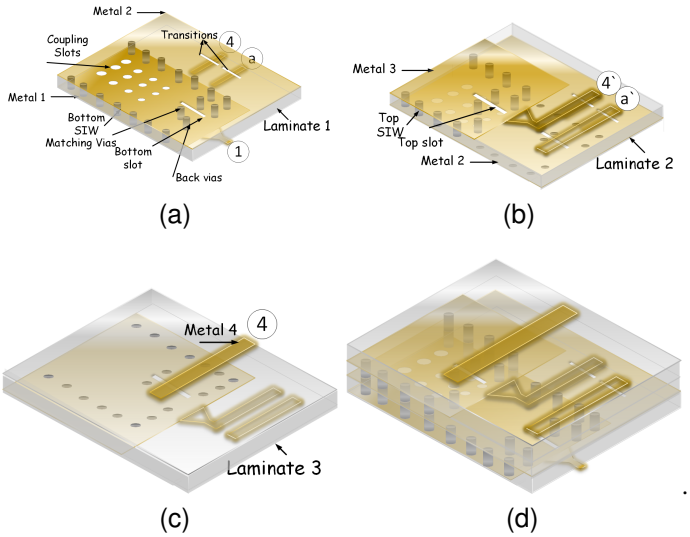

Fig. 2. Layer diagram of the directional coupler's half structure, (a) The first two metal layers (the bottom SIW is sandwiched in between), (b) The second and third metal layers where the top SIW is, (c) The third and fourth metal layers, (d) The full layer stack diagram.

duplex mode division multiplexing by allowing both modes to be operated over the same frequency range. Such multiplexing can further enhance the data rates achievable by single-mode systems or match them at lower center frequencies.

In this article, the work presented in [23] is extended by introducing a new dual-mode directional coupler design. To the best of our knowledge, this is the first realization in the literature of a directional coupler on SIW that can couple two modes concurrently. In order to accommodate more peripheral nodes along the surface of the same SIW channel, a weak coupling level (-10 dB) is employed equally for both modes. This, as well as the significant cross-modal isolation ($>$ 30 dB), allows the construction of a multi-mode multi-drop channel (MMD) link that leverages mode-division multiplexing to extend the channel capacity. The only previous realization of such a link was in [26], where a silicon waveguide was used, and each mode was coupled in a single location using evanescent mode couplers. The proposed design, however, supports dual-mode operation along the SIW from end to end, making both modes available at any point along the link surface. Potential applications of this technology include situations where a head node (e.g., a CPU) must communicate with several peripherals (e.g., memory chips) over the same bus. The CPU node, with the help of the designed coupler, can communicate with the peripherals using the two modes concurrently, enabling two potential strategies: 1) The CPU utilizes both modes as two independent channels, and half of the peripherals listen to each mode, doubling the total number of peripherals that can be on the bus in comparison to traditional single-mode communications as illustrated in Fig. 1. 2) The CPU sends data using one mode, and the peripherals use the other mode to simultaneously transmit data back to the CPU, enabling full-duplex bidirectional communication. Although we demonstrate our prototype at a relatively low-frequency band (10-15 GHz), we provide a detailed frequency-independent design methodology, making it easily scalable to any band of interest. Scaling this design to the THz range, in particular, requires more attention on via size constraints and losses. However, such scaling has been successfully demonstrated in multiple prior works over several sub-THz bands as in [10] and more recently in [24] and [25].

The prototype coupler was fabricated by stacking three laminates of (RT Duroid 5880) with (h = 0.508 mm, ϵ_r = 2.2, $tan\ (\delta) = 0.004$) on top of each other. The half-structure layer diagram is shown in Fig. 2. The two-coupled SIWs are formed between metals (1 and 2) for the bottom and (2 and 3) for the top. For each waveguide, TE_{10} and TE_{20} are excited concurrently. The TE_{10} mode is excited on metals (1 and 3) for the bottom and top SIW, respectively. Additionally, the TE_{20} mode is excited by etching slots on metals (2 and 3) for the bottom and top SIW, respectively. The slots are fed using 50 Ω microstrips on layers (3 and 4), respectively. Since two excitation sources, i.e., Top TE_{10} and Bottom TE_{20} respectively, exist (after assembly) on an internal metal (metal 3), a via-less, broadband vertical transition from this metal to metal one is designed to allow better accessibility of the ports. A block diagram of the design structure as well as the ports labeling are illustrated in Fig. 3. The paper is organized as follows: Section II details the mode excitation and matching techniques, Section III explains the multi-port multi-mode design, Section IV presents the fabricated structure and the results, and Section V presents our concluding remarks.

II. Modes Excitation

This section details more the authors' work in [23] on concurrent excitation of the first two modes of the SIW. The excitation of SIWs is done by maximizing the overlap integral between the excitation source and the modal field profiles. Designing the exciting structure starts by choosing the SIW's width to satisfy a particular cut-off frequency (5 GHz for TE_{10} in this case) as demonstrated in [27], followed by selecting the excitation sources for both modes. Next, matching networks are designed between those sources and the SIW. This section is split into two subsections for describing the modal excitation design methodology: the first deals with the excitation sources, and the second discusses the matching considerations.

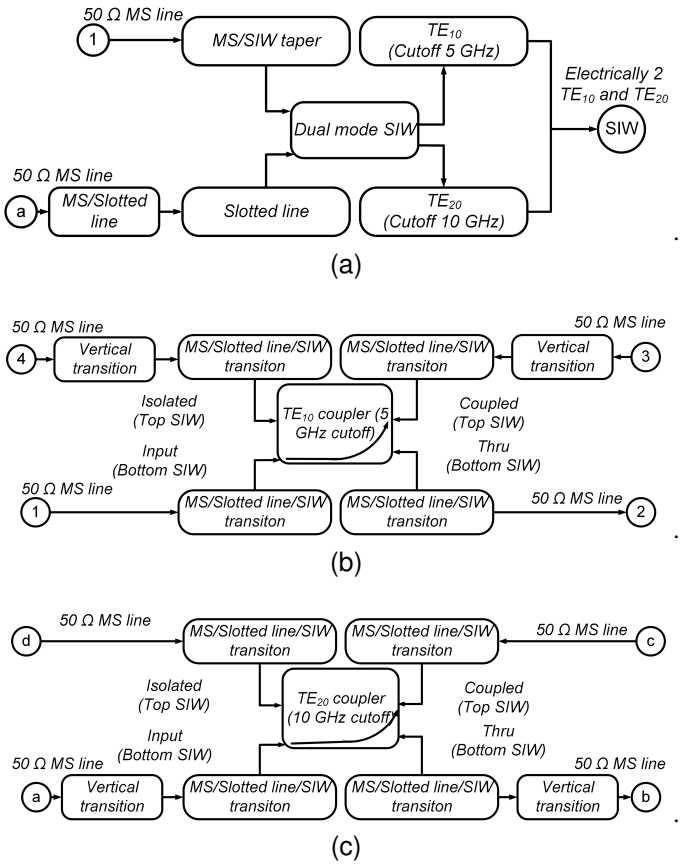

Fig. 3. Block diagrams of the design structures used in this paper: (a) Three-port structure used for exciting both TE_{10} and TE_{20} modes in each of the SIWs (top and bottom). This corresponds to four electrical ports in the circuit model due to the SIW wave port supporting two separate modes. (b) The TE_{10} mode coupler , (c) The TE_{20} mode coupler. Both (b) and (c) include excitation structures and port numbers and placement (i.e., top / bottom SIW). The ports (1-4) and (a-d) are all attached to 50Ω microstrip lines.

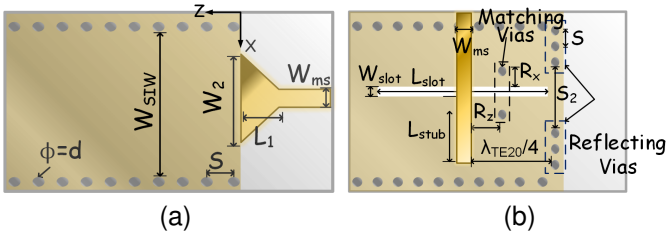

Fig. 4. Diagram of excitation structures for (a) TE_{10} and (b) TE_{20} modes. The axes convention is shown in the first figure.

A. Excitation Sources

Many different approaches for exciting the fundamental mode of SIWs have been proposed previously [28]–[31]. In this design, a 50 Ω microstrip line is adiabatically tapered into the center of the SIW as shown in Fig. 4a. This creates a maximum transverse electric field in the middle of the waveguide resembling that of the fundamental mode, thus maximizing the overlap integral [28]. This excitation is uni-directional since the power is coupled to the far end of the SIW, creating a forward traveling wave.

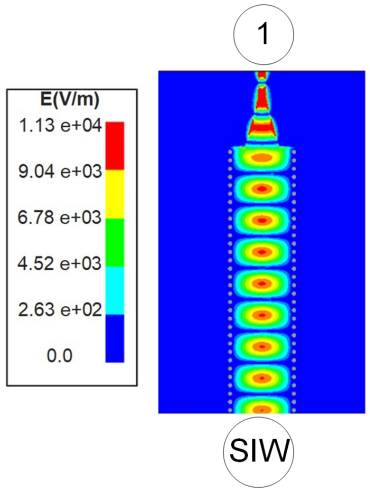

Fig. 5. The simulated TE_{10} mode profile excited by the microstrip to SIW structure. Port 1 excites the microstrip and port SIW is a terminating wave-port

On the other hand, the first higher order mode (TE_{20}) is excited using a slot with infinitesimal width etched longitudinally (along the propagation direction) on the top wall [19] of the waveguide shown in Fig. 4b. A 50 Ω microstrip above the slot on the top layer feeds it. The electric field extends perpendicularly from the top microstrip, i.e., along the Y-direction, as shown in Fig. 4a. According to [18], [32], a slot (with a small width) fed by a perpendicular electric field is polarized creating a null of the electric field in its location. Using the equivalence theorem, this polarization can be treated as an equivalent magnetic current along the slot length (Z-direction) [18], [32]. The exciting slot resonates at half-wavelength, and the magnetic current can be expressed as:

$$M_z = M_0\ \delta(y)\ \delta(x - \frac{W_{SIW}}{2})\ sin(\beta_{slot} z), \qquad (1)$$

where β_{slot} is the wave propagation constant of the slotted line, assuming that the width can be neglected compared to the length. In practice, the width is chosen to be as small as possible to justify the assumption and minimize the insertion loss. Under this approximation, only the H_z component of TE_{20} will contribute to the overlap integral since the other field components are zero when evaluated at ($x = W_{SIW}/2$, i.e., the center of the SIW) [18]. The overlap integrals become:

$$A^+ = \frac{1}{P_{20}} \oint_V |H_z|\ .\ M_z\ e^{-j\beta_{20} z}\ dv \qquad (2)$$

$$A^- = \frac{1}{P_{20}} \oint_V |H_z|\ .\ M_z\ e^{j\beta_{20} z}\ dv \qquad (3)$$

The first integral considers the (+Z) traveling wave, and the second considers the (-Z) one. P_{20} represents the power carried in the mode, H_z is the magnetic field component of the TE_{20} mode in the Z-direction, and β_{20} is the TE_{20} propagation constant in the SIW. Unlike the TE_{10} excitation, which was uni-directional, the TE_{20} excitation is bi-directional. Therefore, to enforce propagation in the positive Z-direction, reflecting vias as shown in Fig 4b are placed at a quarter modal wavelength (λ_{TE20}) away from the center of the slot. These vias prohibit

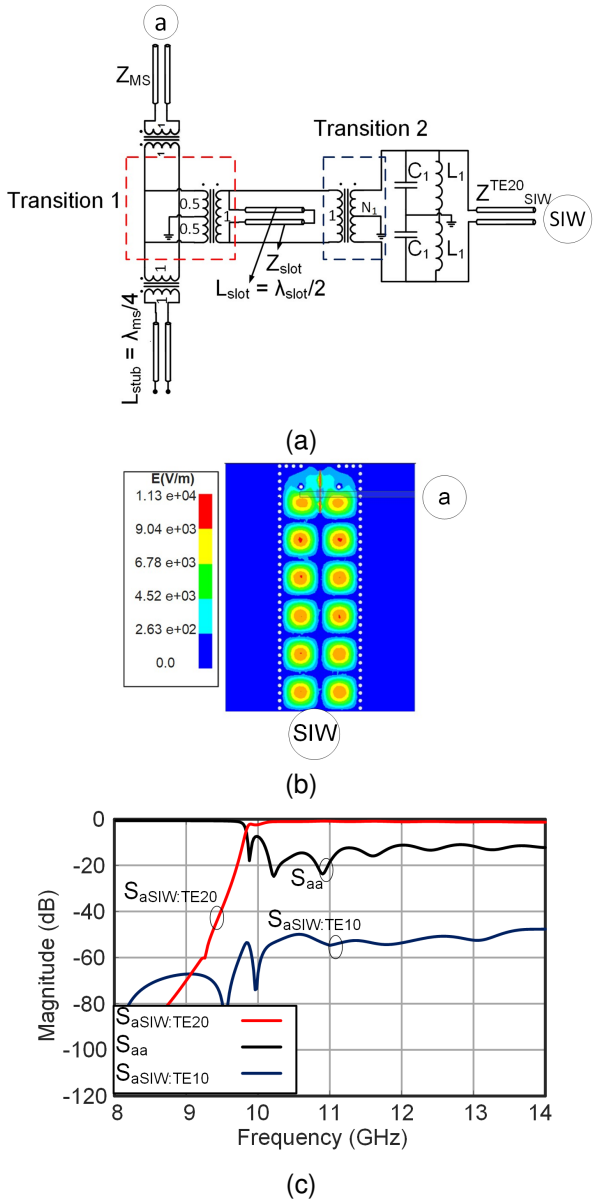

Fig. 6. TE_{20} exciting structure. (a) Equivalent circuit model, (b) Simulated electric field plot excited by microstrip-to-slotline structure, and (c) Simulated S-parameters of the excitation structure (Port a excites the top microstrip feeding the slot and port SIW is a terminating wave port. The convention $SIW : TE_{n0}$ means the TE_{n0} mode of the SIW port).

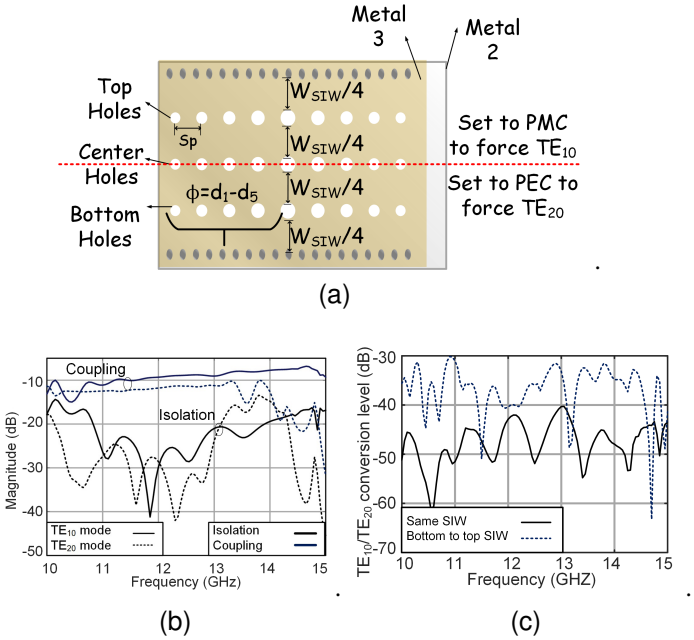

Fig. 7. (a) Diagram of the proposed directional coupler indicating the three rows of holes. (b) Coupling of TE_{10} (S_{13}) and TE_{20} (S_{ac}) modes and Isolation TE_{10}, S_{14}, and TE_{20}, S_{ad}) of each mode coupler, (c) Cross-modal isolation along the same SIW (S_{1a}) and transitioning from bottom to top SIW (S_{1c}). Port numbers are summarized in Fig. 3.

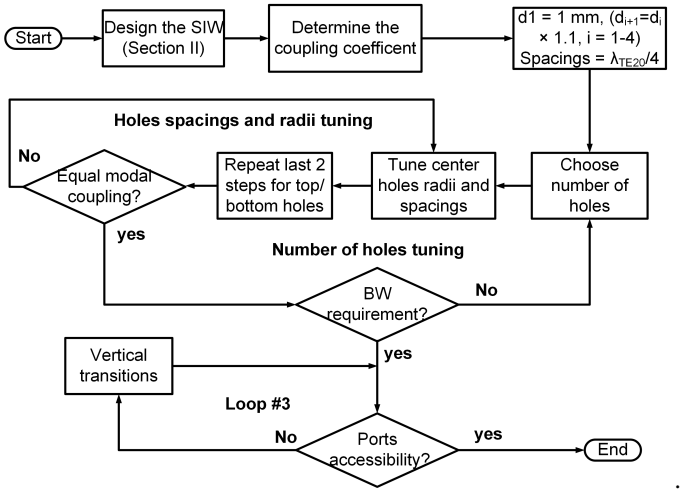

Fig. 8. Flowchart of the proposed design.

propagation in the backward direction. The quarter wavelength separation makes the reflected wave add in phase with the forward traveling one.

B. Matching Considerations

Matching ensures maximum power transfer from the excitation source to the SIW. For the fundamental mode, we aim to match a 50 Ω microstrip to the SIW fundamental mode impedance given by:

$$Z_{TE_{10}} = \frac{K\eta}{\beta_{10}} \tag{4}$$

$$K^2 = \beta_{m0}^2 + K_c^2 \tag{5}$$

$$K_c = \frac{m\pi}{W_{SIW}} \tag{6}$$

where $K = \omega\sqrt{\mu_0\epsilon_r\epsilon_0}$ is the plane-wave propagation constant in the dielectric, β_{10} is the fundamental mode-guided propagation constant, and $\eta = 254.17\ \Omega$ is the plane wave propagation impedance in the dielectric. The relationship between K and β_{m0} is given in (5), and $K_c = m \times 147.5\ m^{-}1$ is the cut-off propagation constant for any mode m (m = 1 for the fundamental mode). The design starts by designing a 50 Ω microstrip; the modal impedance can be evaluated from (4). A certain taper length and width (L_1 and W_2 in Fig4a) are chosen and tuned for the required response [28]. The excited mode profile is shown in Fig. 5.

Subsequently, the excitation structure of the TE_{20} mode,

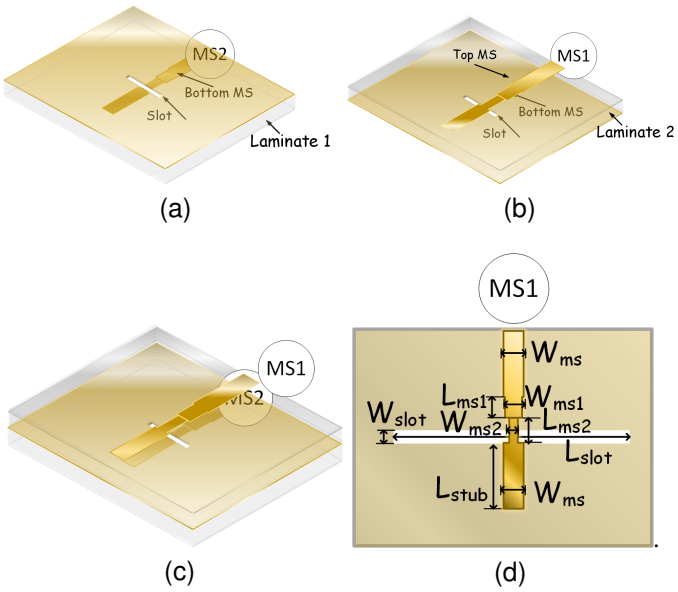

Fig. 9. Diagram of the proposed via-less vertical transition. (a) The first two metal layers, (b) The second and third metal layers, (c) Full layer diagram, (d) Top view of the proposed transition with length and width parameter labels.

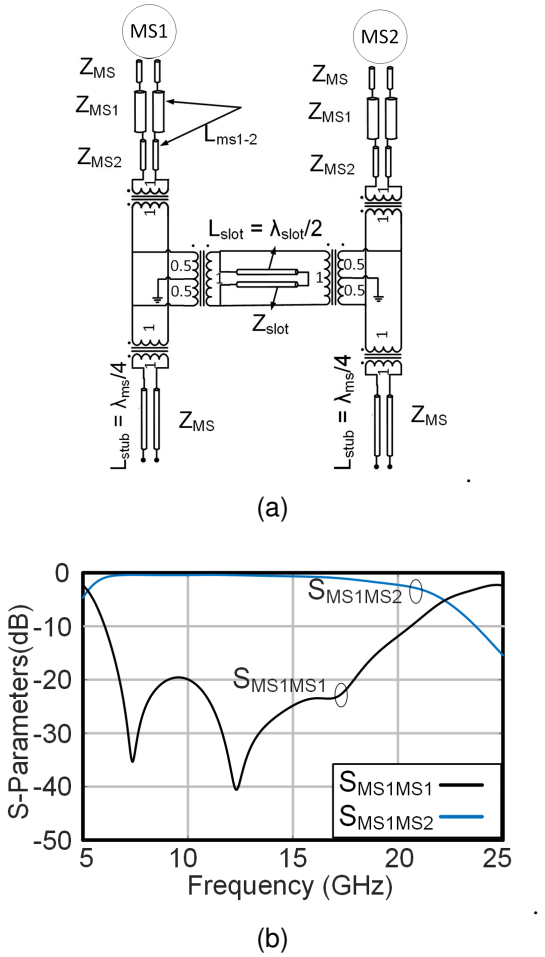

Fig. 10. (a) Equivalent circuit model of the the proposed via-less vertical transition. (b) EM simulated S-parameters.

shown in Fig. 4b, can be modeled with the equivalent circuit model shown in Fig. 6a. The circuit model can be divided into two parts. The first part is the microstrip/slotted line transition, where port (a) represents the input microstrip, and the junction at the microstrip/slotted line intersection is modeled by the microstrip (1:1) transformer connected to the slotted line center-tapped (0.5:1) transformer [35]. A quarter wavelength (at the frequency of interest) open stub is added to the top microstrip to improve matching. The frequency of interest is usually chosen to be at the center of the design band. On the other hand, the length of the slotted line is chosen to be half a slotted line wavelength at the same frequency.

The second part of the circuit model is a slotted line/SIW transition that can be designed as in [19], where the input impedance of the TE_{20} mode is evaluated using (4 - 6) by setting m = 2 in (6) and replacing each β_{10} with β_{20} in (4). The SIW's capacitive input impedance nature is modeled by C_1 in the equivalent circuit model. Two thru-vias, modeled as inductors (L_1) as shown in Fig. 6a, are used for matching. Adjusting the via distances from the slotted line (R_x and R_z) in Fig. 4b affects the equivalent SIW impedance seen by the slotted line improving matching. Unfortunately, these vias also affect the TE_{10} matching, requiring careful concurrent dual-mode matching. This can be done by fine-tuning the vias' positions. A good starting point is to select R_x to be more than $0.5 \times W_2$ as shown in Fig. 4. This way, the effect on the taper matching of the fundamental mode is minimal. On the other hand, R_z is tuned to enhance the matching. A reasonable rule of thumb is to start with R_z that place the posts as close as possible to the exciting microstrip line. The resulting S-parameters of the excitation structure in Fig. 6b are shown in Fig. 6c. The mode is excited with low-insertion loss and cross-modal coupling below -40 dB for the fundamental mode (TE_{10}).

III. Multi-port Multi-mode Design

The authors originally proposed concurrent multi-mode end-to-end links in [23]. Since many communication links may require multiple devices to be interconnected on the same bus, a natural extension for the previous work is a multi-mode multi-port link over an SIW. To that end, a concurrent dual-mode multi-hole SIW directional coupler is designed to achieve the multi-port operation. To our knowledge, this is the first demonstration of a concurrent dual-mode SIW directional coupler. This section details the coupler design and deals with some potential design issues.

A. Multi-Mode Multi-Hole Coupler Design

SIW directional couplers have been proposed in multiple forms for single-mode operation [11]–[16]. We are only aware of waveguide-based dual-mode couplers existing for bulky 3D waveguides, which use the TE_{10} and TE_{01} modes [36]–[40]. This work proposes the first concurrent dual-mode, TE_{10} and TE_{20} SIW directional coupler. It is a (-10dB) multi-hole coupler in which two waveguides are placed on top of each other, as shown in Fig 2. Three sets (top, center, and bottom) of circular coupling holes are etched out in the common wall (metal 2) as shown in Fig. 7a. Choosing the number of holes,

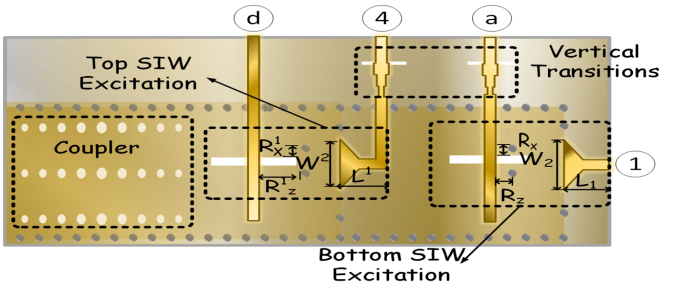

Fig. 11. Diagram of one half of the SIW link showing 4 of the 8 total ports in the system and the dual-mode excitation structures. Ports 1 and a drive the mode 1 and 2 end launchers respectively and ports 4 and d connect to the mode 1 and 2 launchers on one end of the directional coupler.

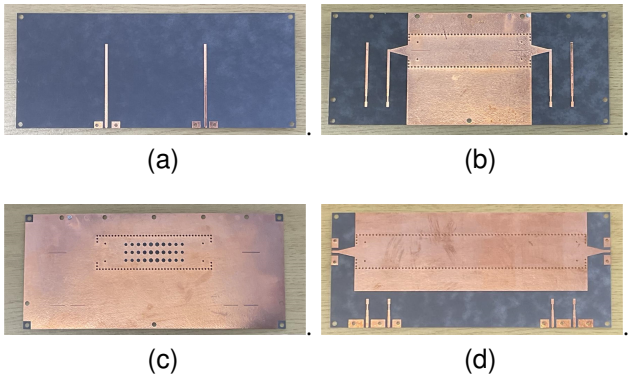

Fig. 12. The fabricated PCBs before assembly. (a) Layer 1, (b) Layer 2, (c) Layer 3, and (d) Layer 4.

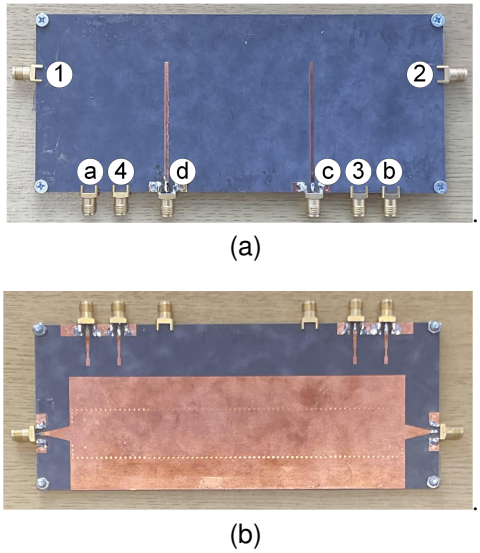

Fig. 13. Fabricated SIW system after assembly. (a) Top layer, (b) Bottom layer.

their diameters (d_1 - d_5), and spacings (Sp) controls both coupling and operation bandwidth as discussed in [41].

Interestingly, in this design, each of the three sets of holes affect the coupling of the two modes differently, enabling designing the coupling coefficients for the two modes separately. To see this effect, the SIW coupler is simulated (with wave ports on both sides) by cutting it into two halves and terminating it with a perfectly magnetic/electric conductor (PMC / PEC) boundary to force (TE_{10} / TE_{20}) operation respectively as illustrated in Fig. 7a. Unlike, the small-width slot in Section II, the round holes can be polarized both electrically and magnetically with different values from the bottom SIW field components. The transverse components (E_y and H_x) of the TE_{10} mode in the bottom SIW are at their maxima in the center. Thus, they contribute the most to the center holes' equivalent electric/magnetic current. Conversely, the TE_{20} transverse fields are null at the center, so the only contribution to the equivalent currents comes from the longitudinal H_z component. On the other hand, the top and bottom holes are positioned such that the TE_{20} transverse fields are at their maxima, while the TE_{10} ones are not. Nevertheless, the TE_{10} transverse fields still contribute to the equivalent current since they are not completely zero at the locations of the top and bottom holes. These simulations also reveal that the center holes cannot efficiently couple into TE_{10} mode; however, they are the most effective ones for exciting TE_{20} since the field configuration of the holes matches the modal profile of the center slots, as discussed in the previous section. However, the equivalent currents on the center holes come from both TE_{10} and TE_{20} modes. This implies a certain level of cross-modal conversion from TE_{10} to TE_{20} mode going from the bottom SIW to the top. On the other hand, the top and bottom holes can couple both modes at the same time but they are more effective for TE_{10} mode coupling. A more detailed mathematical treatment of the holes' equivalent currents and coupling factors is given in Appendix I.

The design procedure starts by choosing the required coupling factor based on the number of drop ports required along the link. In this realization, the coupling factor was chosen to be -10 dB, enabling up to around 10 peripheral devices to coexist along the channel. The multi-drop realization scheme for communicating with multiple peripheral nodes can be realized by cascading several instances of the proposed coupler along the surface of the main SIW. The next step is choosing the number of holes to match the FBW requirement of the coupler. Following this, progressive sizing and spacings for those holes are chosen. An initial design step suggested by [41] is to select the spacings to be ($\lambda_{TE20}/4$) for the center row, and ($\lambda_{TE10}/4$) for the other rows. The diameters ($d_1 - d_5$) are chosen to increase progressively by a factor of 1.1; usually for the required small coupling, they should be chosen to be small (e.g., $d_1 = 1\ mm$). The holes' spacings and their diameters are then engineered to achieve a relatively equal coupling for both modes. In this realization, the goal was to achieve roughly equal (-10 dB) for both the TE_{10} and TE_{20} modes, as shown in Fig. 7b. This equal division is intended for being able to fully utilize both modes for multiplexing peripheral nodes along the link with a 15-dB bandwidth for both modes greater than 4 GHz. The coupling and isolation (same mode and cross-modal) results of the coupler are shown in Fig. 7b and 7c. It is apparent that the cross-modal isolation degrades going from bottom to top SIW, confirming the presented coupling theory. The full design procedure is summarized in the flow chart, Fig. 8.

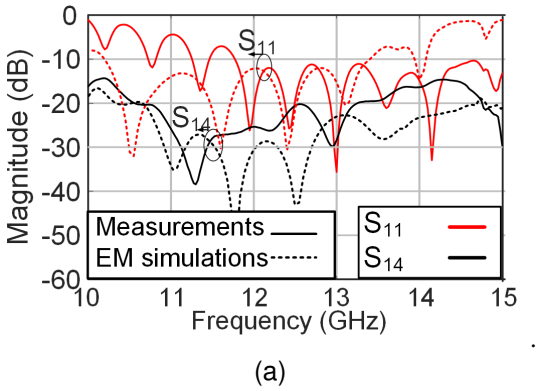

(a)

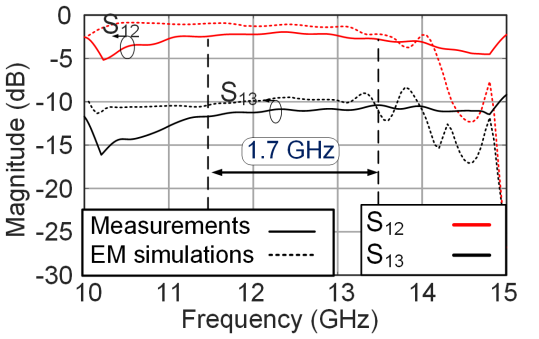

(b)

Fig. 14. TE_{10} mode directional coupler measurement data: (a) Return Loss and Isolation, (b) Thru and Coupling. Markers are added to highlight the 1.7 GHz of concurrent BW for MDM.

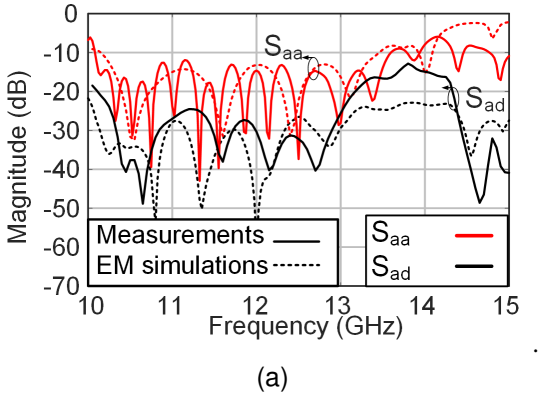

(a)

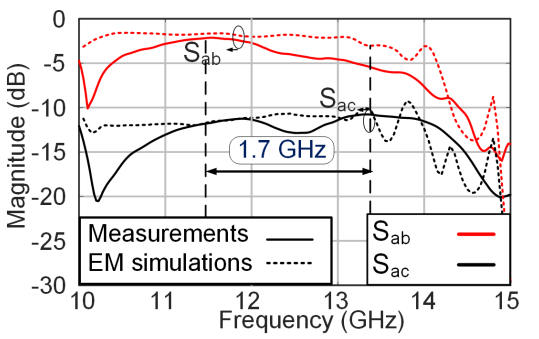

(b)

Fig. 15. TE_{20} mode directional coupler measurement data: (a) TE_{20} Return Loss and Isolation, (b) Thru and Coupling. Markers are added to highlight the 1.7 GHz of concurrent BW for MDM.

B. Excitation Ports Accessibility

The proposed structure consists of four stacked metal layers, as illustrated in Fig. 2. In this figure, there are two excitation sources (denoted by 4‘ and a‘) on metal 3, which correspond to the bottom TE_{20} excitation and the top TE_{10} excitation). After fabrication and assembly, these sources are inaccessible by SMA connectors, which must have their center signal pin attached to a conductor on the top or bottom layers. A vertical transition from metal 3 to metal 1 is designed to resolve this issue. The required transition must have a much larger bandwidth than the couplers not to affect the overall performance. A via is the simplest vertical transition, but it, unfortunately, has a low pass response. Hence, vias are not often used for high-frequency, wideband applications. Several vertical transitions have been proposed in the literature, using via, as in [33], or via-less transitions, as in [34]. Following the work in [34], a slotted line-based transition is designed.

The proposed transition consists of three metal layers, as depicted in Fig. 9. The first metal consists of an input microstrip coupled to a slot on the second layer. The slot is then coupled to another microstrip on the bottom layer. This is known as a microstrip-slotted line-microstrip transition. A stepped impedance resonator is designed to help with matching at the input and output, enhancing the bandwidth for broadband operation. The transition schematic is shown in Fig 9d. The equivalent circuit model of this structure can be derived from the model proposed in [35] as shown in Fig. 10a.

The circuit model is optimized for wideband matching and transmission. The optimized circuit parameters are then fed to the EM simulator as an initial design starting point. In the EM simulation, the transition is simulated along with the full remaining structure of the SIW, and fine-tuning is applied to account for non-idealities caused by the upper microstrip being covered with another substrate and metal layer on top. The EM simulation results of the transition are shown in Fig 10b. The 10-dB return loss (RL) bandwidth is roughly 15 GHz (from 5-20). This is significantly larger than the directional coupler, so the transition can be safely incorporated without noticeably affecting the overall performance.

IV. Measurement Results

The proposed waveguide coupling system consists of 8 ports (4 nodes with two ports for each mode). The structure is symmetric, and the schematic of the half structure (directional coupler and transitions) is shown in Fig. 11. The ports labeled (1-4) are the TE_{10} exciting ports, where 1 is the input port, 2 and 3 are the thru and coupled ports, respectively, and 4 is the isolation port. On the other hand, lower-case letters are used to label the ports associated with the TE_{20} mode, where a is the input port, b, and c are the thru and coupled ports, respectively, and d is the isolation port. The dimensions of the proposed structure, shown in Figs. 4, 7a. 9 and 11, are summarized in table I.

The structure is fabricated by stacking three laminates of (RT Duroid 5880) with (h = 0.508 mm, $\epsilon_r = 2.2$, $tan\ (\delta) =$

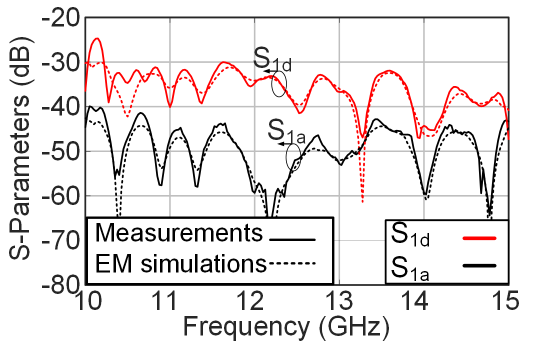

(a)

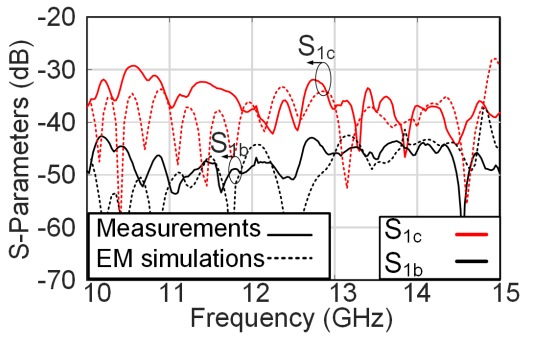

(b)

Fig. 16. Cross-modal Isolation (a) S_{1a} and S_{1d}, (b) S_{1b} and S_{1c}

.

TABLE I
DIMENSIONS OF THE FABRICATED STRUCTURE

Parameter	Length (mm)
d	1 mm
d_1	2 mm
d_2	2.16 mm
d_3	2.3 mm
d_4	2.5 mm
d_5	2.7 mm
L_1	10 mm
L^1	10.3 mm
L_{ms1}	4.7 mm
L_{ms2}	3.6 mm
L_{slot}	13 mm
L_{stub}	5.4 mm
R_z	5.7 mm
R_z^1	5.9 mm
R_x	6 mm
R_x^1	5.8 mm
S	1 mm
S_2	10 mm
Sp	2 mm
W_2	6.5 mm
W^2	7.1 mm
W_{ms}	1.6 mm
W_{ms1}	1.25 mm
W_{ms2}	0.8 mm
W_{SIW}	21.3 mm
W_{ms}	1.6 mm
W_{slot}	0.3 mm

0.004) on top of each other. In this prototype, the laminates are attached together using screws and bolts, although they could

TABLE II
COMPARISON AGAINST PRIOR WORK

	Elec.Lett-'11 [12]	MWCL-'17 [13]	MOTL-'14 [14]	EUMC-'10 [15]	TMTT-'13 [16]	**This Work**
Modes	TE_{10}					TE_{10} **and** TE_{20}
Freq.	(10-15)	(26-40)	(8-12)	(13-15)	(8-11)	**(10-15)**
10-dB RL FBW (%)	N/A[1]	>35.2[2]	12	14	16	**32/35**[3]
IL (dB)	0.7	0.4	2	2	1.6	**1/1.5**
Cross-modal Coupling	N/A					**(40/30)**
Coupling level	-6	-20	-10	-3		**-10/ -10**
MMD	No					**Yes**
Coupler type	Multi-hole			Riblet		Multi-hole

[1] S_{11} is over 10-dB. [2] 20-dB RL FBW.
[3]FBW is calculated with respect to the cut-off frequency of TE_{20} (10 GHz).

otherwise be held together using epoxy. The fabricated structure before and after assembly is shown in Figs. 12 and 13, respectively. The reference plane of the measurements is the endpoint of the SMA connectors, with only the VNA ports and cables de-embedded, so the overall insertion-loss includes losses from the connectors and soldering. The RL/isolation results for the TE_{10} excitation are illustrated in Fig 14a. The 10-dB RL/isolation BW is more than 3.2 GHz (11.8 - 15 GHz). The thru/coupling performance of the coupler for the TE_{10} mode is illustrated in Fig. 14b, confirming that the coupling is roughly flat at 10 dB for 4 GHz (11 - 15 GHz) of bandwidth. The insertion loss in the measured result compared to EM simulations is approximately 0.5 dB below 10 dB. This can be attributed to potential misalignment due to the laminates being stacked using screws and nuts and losses due to soldering and the connector.

The TE_{20} coupling results are illustrated in Figs 15a and 15b. The 10-dB RL/isolation BW is roughly 3.5 GHz (10 - 13.5 GHz). This provides 1.7GHz of available bandwidth for full-duplex mode division multiplexing. The coupling is approximately 10dB with 1.5dB insertion loss (IL). The additional 0.5 dB insertion loss can be attributed to the slot excitation requiring the exact alignment of the layers and the loss of the slot itself. The cross-modal isolation across the bottom SIW (S_{1a} and S_{1b}), as well as that from transitioning from the bottom to the top SIW (S_{1c} and S_{1d}), are shown in Fig. 16. The isolation along the same SIW is greater than 40 dB from 10 - 15 GHz, which is roughly 10 dB more than the isolation of two side-by-side waveguides having (1 mm) pitch between vias [23]. The cross-modal isolation from bottom to top is around 30dB (10dB less than across the same SIW confirming that some cross-modal conversion occurs going from bottom to top) across the same range. The work is distinct compared to all prior work since the two modes are excited and coupled at the same time. Nevertheless, a comparison against

other state-of-the-art SIW directional couplers is given in Table II. As can be seen in the comparison table, the proposed structure compares favorably against prior work despite being able to additionally handle two modes concurrently.

V. Conclusion

This paper presented a concurrent dual-mode directional coupler in SIW technology for the first time. The coupler enables the realization of dual-mode multi-drop channel links, which can leverage mode-division multiplexing to enhance the overall data rate. The concurrency of the frequency bands of the two modes allows for easier transceiver design for a true full-duplex channel link. The structure is fabricated by stacking three laminates vertically and aligning them using screws. The modes are excited concurrently in a 1.7 GHz(11.8-13.5 GHz) band with low insertion loss and high cross-modal isolation. Measurements for the fabricated structure agree well with EM simulations confirming the theoretical predictions and opening doors to a multi-mode multi-drop system realization over substrate-integrated waveguides.

Appendix
Derivation of the coupler's equivalent currents and holes' coupling factors

The derivation starts realizing that the aperture's normal electric and tangential magnetic fields create field lines that resemble a normal electric polarization current and a tangential magnetic polarization current [18]. The polarizability of a hole with a diameter (d) is given as: [18]

$$\alpha_e = \frac{d^3}{12} \tag{7}$$

$$\alpha_m = \frac{d^3}{6} \tag{8}$$

Based on this polarizability, the modal electric and magnetic fields of each of the two operating modes induce equivalent electric and magnetic currents in the holes [18] as given in the following equations:

$$J_y = \epsilon_0 \alpha_e |E_{yn0}|_{(x_0,b)} sin(\frac{2\pi s}{d}) \delta(x-x_0)\delta(y-b)\delta(z-z_0) \tag{9}$$

$$M_x = \frac{\alpha_m}{Z_{n0}} |H_{xn0}|_{(x_0,b)} sin(\frac{2\pi s}{d}) \delta(x-x_0)\delta(y-b)\delta(z-z_0) \tag{10}$$

$$M_z = -\frac{2j\pi\alpha_m}{\beta d\ Z_{n0}} |H_{zn0}|_{(x_0,b)} cos(\frac{2\pi s}{d}) \delta(x-x_0)\delta(y-b)\delta(z-z_0) \tag{11}$$

where x_0 is the hole position in the X-direction ($W_{SIW}/4$ for the top, $W_{SIW}/2$ for the center, and $3W_{SIW}/4$ for the bottom), b is the height of the SIW, and z_0 is the hole position in the Z-direction. The subscript (n0) refers to the mode, whether (10) or (20). The total equivalent electric or magnetic current is the summation of the contribution of both excited modes (10) and (20). Each one of the holes acts as a source that emits fields into the upper SIW. These fields can be evaluated using overlap integrals of the equivalent sources with the modal fields as follows:

$$A^+ = \frac{-1}{P_{n0}} \oint_V |E^-_{no}| \ . \ J \ dv + \frac{1}{P_{n0}} \oint_V |H^-_{no}| \ . \ M \ dv \tag{12}$$

$$A^- = \frac{-1}{P_{n0}} \oint_V |E^+_{no}| \ . \ J \ dv + \frac{1}{P_{n0}} \oint_V |H^+_{no}| \ . \ M \ dv \tag{13}$$

The equivalent field in the positive direction (F) is the summation of the contribution of each hole given the relative phase differences:

$$F = \sum_{m=1}^{3} \sum_{n=1}^{N} A^+_{m,n} e^{-j\Delta\phi_{nx}} e^{-j\Delta\phi_{mz}} \tag{14}$$

$$B = \sum_{m=1}^{3} \sum_{n=1}^{N} A^-_{m,n} e^{-j\Delta\phi_{nx}} e^{j\Delta\phi_{mz}} \tag{15}$$

where (m) is the column number (top, middle, and bottom), $\Delta\phi_{nx,mz}$ are the relative phase differences between holes in the x and z directions respectively, and (n) loops over the holes in the same column. The coupling thus corresponds to the forward wave amplitude in comparison to the input and the directivity is the backward wave over the forward one as given in [18].

References

[1] C. A. Thraskias et al., "Survey of Photonic and Plasmonic Interconnect Technologies for Intra-Datacenter and High-Performance Computing Communications," *IEEE Commun. Surveys Tut.*, vol. 20, no. 4, pp. 2758-2783.

[2] J. W. Holloway, G. C. Dogiamis and R. Han, "Innovations in Terahertz Interconnects: High-Speed Data Transport Over Fully Electrical Terahertz Waveguide Links," *IEEE Microw Mag.*, vol. 21, no. 1, pp. 35-50, Jan. 2020.

[3] J. W. Holloway, L. Boglione, T. M. Hancock, and R. Han, "A fully integrated broadband sub-mmWave chip-to-chip interconnect," *IEEE Trans. Microw. Theory Techn.*, vol. 65, no. 7, pp. 2373–2386, 2017.

[4] Q. J. Gu, "THz interconnect: The last centimeter communication," *IEEE Commun. Mag.*, vol. 53, no. 4, pp. 206–215, 2015.

[5] J.-H. Lee, N. Kidera, G. DeJean, S. Pinel, J. Laskar, and M. M. Tentzeris, "A V-band front-end with 3-D integrated cavity filters/duplexers and antenna in LTCC technologies," *IEEE Trans. Microw. Theory Techn.*, vol. 54, no. 7, pp. 2925–2936, Jul. 2006.

[6] K. Dhwaj, Y. Zhao, R. A. Hadi, X. Li, F. M.-C. Chang, and T. Itoh, "A 0.55 THz on-chip substrate integrated waveguide antenna," in *Proc. 43rd Int. Conf. Infr., Millim., Terahertz Waves (IRMMW-THz)*, Sep. 2018, pp. 6–7.

[7] Y. J. Cheng, W. Hong, and K. Wu, "Design of a monopulse antenna using a dual V-type linearly tapered slot antenna (DVLTSA)," *IEEE Trans. Antennas Propag.*, vol. 56, no. 9, pp. 2903–2909, Sep. 2008.

[8] Y. Shang, H. Yu, H. Fu, and W. M. Lim, "A 239–281 GHz CMOS receiver with on-chip circular-polarized substrate integrated waveguide antenna for sub-terahertz imaging," *IEEE Trans. THz Sci. Technol.*, vol. 4, no. 6, pp. 686–695, Nov. 2014.

[9] K. Sakakibara, Y. Kimura, A. Akiyama, J. Hirokawa, M. Ando, and N. Goto, "Alternating phase-fed waveguide slot arrays with a single-layer multiple-way power divider," in *IEE Proc.-Microw., Antennas Propag.*, vol. 144, no. 6, pp. 425–430, Dec. 1997.

[10] J. W. Holloway, G. C. Dogiamis, S. Shin and R. Han, "220-to-330-GHz Manifold Triplexer With Wide Stopband Utilizing Ridged Substrate Integrated Waveguides," *IEEE Trans. Microw. Theory Techn.*, vol. 68, no. 8, pp. 3428-3438, Aug. 2020.

[11] K. -S. Chin, C. -C. Chang, C. -H. Chen, Z. Guo, D. Wang and W. Che, "LTCC Multilayered Substrate-Integrated Waveguide Filter With Enhanced Frequency Selectivity for System-in-Package Applications," *IEEE Trans Compon Packaging Manuf Technol* ., vol. 4, no. 4, pp. 664-672, April 2014.

[12] A. A. M. Ali, H. B. El-Shaarawy and H. Aubert, "Compact wideband double-layer half-mode substrate integrated waveguide 90°deg coupler," *Electron. Lett.*, vol. 47, no. 10, pp. 598-599, May 12 2011.

[13] A. Doghri, T. Djerafi, A. Ghiotto and K. Wu, "Substrate Integrated Waveguide Directional Couplers for Compact Three-Dimensional Integrated Circuits," *IEEE Trans. Microw. Theory Techn.*, vol. 63, no. 1, pp. 209-221, Jan. 2015.

[14] Moustapha Mbaye, Larbi Talbi, Khelifa Hettak, "Design of a multilayered six-aperture directional coupler using substrate integrated waveguide", *Microw. Optical Techn. Lett.*, vol.56, no.1, pp.23, 2014.
[15] F. Carrera, D. Navarro, M. Baquero-Escudero and V. M. Rodrigo-Peñarrocha, "Compact substrate integrated waveguide directional couplers in Ku and K bands," *in Proc. Eur. Microw. Conf* (EuMC), Paris, France, 2010, pp. 1178-1181.
[16] F. Alessandri, M. Giordano, M. Guglielmi, G. Martirano and F. Vitulli, "A new multiple-tuned six-port Riblet-type directional coupler in rectangular waveguide," *IEEE Trans. Microw. Theory Techn.*, vol. 51, no. 5, pp. 1441-1448, May 2003.
[17] S. Liu and F. Xu, "Compact Multilayer Half Mode Substrate Integrated Waveguide 3-dB Coupler," *IEEE Microw. Wireless Comp. Lett.*, vol. 28, no. 7, pp. 564-566, July 2018.
[18] D. M. Pozar, *Microwave Engineering*, 3rd ed. New York, NY, USA: Wiley, 2005.
[19] P. Wu, J. Liu, and Q. Xue, "Wideband excitation technology of TE20 mode substrate integrated waveguide (SIW) and its applications," *IEEE Trans. Microw. Theory Techn.*, vol. 63, no. 6, pp. 1863–1874, Jun. 2015.
[20] A. Suntives and R. Abhari, "Design and application of multimode substrate integrated waveguides in parallel multichannel signaling systems," *IEEE Trans. Microw. Theory Techn.*, vol. 57, no. 6, pp. 1563–1571, Jun. 2009.
[21] P. Wu, S. Liao and Q. Xue, "Wideband Excit1ations of Higher-Order Mode Substrate Integrated Waveguides and Their Applications to Antenna Array Design," *IEEE Trans. Antennas Prop.*, vol. 65, no. 8, pp. 4038-4047, Aug. 2017
[22] Sun, L., Zhang, Y., Cai, Y. and Qian, Z. (2017), Wideband excitation technology of substrate integrated waveguide TE30 mode and its antenna application. *Electron. Lett.*, 53: 828-830.
[23] Mohamed. H. A. Elsawaf and Constantine Sideris, "Concurrent Multi-Mode Excitation for Mode Division Multiplexing over Substrate Integrated Waveguide," in *Proc. IEEE MTT-S Int. Microw. Symp.,* San Diego, CA USA, 2023.
[24] S. K. Thapa et al., "Implementation of SIW Cavity in Commercial CMOS Technology for Sub-Terahertz Band Applications," in *Proc. IEEE MTT-S Int. Microw. Symp.,* San Diego, CA USA, pp. 493-496.
[25] R. K. Pokharel et al., "200 GHz-band Low-loss Half-Mode SIW CMOS Interconnects and Transmission Lines for Sub-Terahertz Frequency Band Applications," in *Proc. IEEE MTT-S Int. Microw. Symp.,* San Diego, CA USA, pp. 497-500.
[26] X. Ding, H. Yu, S. Sabbaghi and Q. J. Gu, "G-Band Mode-Coupler-Based Si Dielectric Waveguide for Multidrop Sub-THz Interconnect," *IEEE Microw. Wireless Techn. Lett.*, vol. 33, no. 6, pp. 647-650, June 2023.
[27] H. Uchimura, T. Takenoshita, and M. Fujii, "Development of a 'laminated waveguide'," *IEEE Trans. Microw. Theory Techn.*, vol. 46, no. 12, pp. 2438–2443, Dec. 1998.
[28] D. Deslandes and K. Wu, "Integrated microstrip and rectangular waveguide in planar form," *IEEE Microw. Wireless Comp. Lett.*, vol. 11, no. 2, pp. 68-70, Feb. 2001.
[29] F. Taringou, D. Dousset, J. Bornemann, and K. Wu, "Broadband CPW feed for millimeter-wave SIW-based antipodal linearly tapered slot antennas," *IEEE Trans. Antennas Propag.*, vol. 61, no. 4, pp. 1756–1762, Apr. 2013.
[30] K. Kim, J. Byun, and H. Y. Lee, "Substrate integrated waveguide quasi Yagi antenna using SIW-to-CPS transition for low mutual coupling," in *IEEE AP-S Int. Symp. Dig.*, Jul. 2010, pp. 1–4.
[31] D. Deslandes and K. Wu, "Analysis and design of current probe transition from grounded coplanar to substrate integrated rectangular waveguides," *IEEE Trans. Microw. Theory Techn.*, vol. 53, no. 8, pp. 2487–2494, Aug. 2005.
[32] R. E. Collin, Foundations for Microwave Engineering, 2nd edition, Wiley–IEEE Press, Hoboken, N.J., 2001.
[33] F. P. Casares-Miranda, C. Viereck, C. Camacho-Penalosa and C. Caloz, "Vertical microstrip transition for multilayer microwave circuits with decoupled passive and active layers," *IEEE Microw. Wireless Comp. Lett.*, vol. 16, no. 7, pp. 401-403, July 2006.
[34] X. Huang and K. -L. Wu, "A Broadband and Vialess Vertical Microstrip-to-Microstrip Transition," *IEEE Trans. Microw. Theory Techn.*, vol. 60, no. 4, pp. 938-944, April 2012.
[35] A. M. H. Nasr, A. M. E. Safwat and H. Elhennawy, "Via-free microstrip to slotted line baluns using slotted microstrip cross-junction," *in Proc. Eur. Microw. Conf. (EuMC), 2017*, pp. 85-88.
[36] F. Alessandri and R. Ravanelli, "A new class of dual-mode directional couplers for compact dual-polarization beam-forming networks," *IEEE Microw.Guided Wave Lett.*, vol. 7, no. 9, pp. 300-301, Sept. 1997.
[37] F. Alessandri, M. Dionigi, R. Ravanelli, L. Vanni, "Enhanced dual polarization directional coupler for dual polarization beam forming networks", in *Proc. IEEE MTT-S Inter. Microw. Symp. Digest*, vol.3, pp.1315-1318 vol.3, 2000.
[38] Nelson J. G. Fonseca, Daniele Petrolati, Piero Angeletti, "Design of a waveguide dual-mode three-way power divider for dual-polarization beam forming networks at Ka-band," in *Proc. IEEE Antennas Prop. Society Int. Symp. (APSURSI)*, pp.1096-1097, 2013.
[39] J. L. Cano, A. Mediavilla, S. Dragas and A. Tazón, "Novel Broadband Circular Waveguide Four-Way Power Divider for Dual Polarization Applications," *IEEE Microw. Wireless Compon. Lett.*, vol. 26, no. 2, pp. 98-100, Feb. 2016.
[40] N. J. G. Fonseca, "Broadband Waveguide Dual-Polarization Four-Way Power Divider for Small Passive Arrays," *IEEE Microw. Wireless Compon. Lett.*, vol. 31, no. 8, pp. 985-988, Aug. 2021.
[41] R. Levy, "Analysis and Synthesis of Waveguide Multiaperture Directional Couplers," *IEEE Trans. Microw. Theory Techn.*, vol. 16, no. 12, pp. 995-1006, Dec. 1968.

Mohamed Elsawaf received the B.Sc. and M.Sc. degrees (Hons.) in electrical engineering from Ain Shams University, Cairo, Egypt, in 2018 and 2021, respectively. After graduating, he worked as a software development engineer in the device modeling team at Siemens Digital Industries Software (formerly: Mentor Graphics) for 3 years. During the same time, he worked as a research assistant in the microwave and antenna research lab (MARL) at Ain Shams University. He is currently pursuing a Ph.D. degree at the Department of Electrical and Computer Engineering, University of Southern California (USC), Los Angeles, CA, USA. His research interests include passive and active microwave and THz components for communications and biomedical applications. Mr. Elsawaf was a recipient of the USC Graduate Research Fellowship in 2021.

Constantine Sideris received the B.S., M.S., and Ph.D. degrees (Hons.) from the California Institute of Technology (Caltech), Pasadena, CA, USA, in 2010, 2011, and 2017, respectively. He was a Visiting Scholar with the Berkeley Wireless Research Center, Berkeley, CA, from 2013 to 2014. He was a Post-Doctoral Scholar with the Department of Computing and Mathematical Sciences, Caltech, from 2017 to 2018, working on integral equation methods for electromagnetics. He is currently an Assistant Professor of Electrical and Computer Engineering with the University of Southern California, Los Angeles, CA. His research interests include RF and millimeter-wave integrated circuits for bioelectronics and wireless communications, applied electromagnetics, and computational electromagnetics for antenna design and nanophotonics. Dr. Sideris was a recipient of the ONR YIP Award in 2023, the NSF CAREER Award in 2021, the AFOSR YIP Award in 2020, the Caltech Leadership Award in 2017, and the NSF Graduate Research Fellowship in 2010.